Electronic Supplementary Material (ESI) for Environmental Science: Nano.
This journal is © The Royal Society of Chemistry 2023

# Supporting Information

# Biomass-derived 3D hierarchical Zr-based tubular magnetomotors with peroxidase-like property for selective colorimetric detection and specific decontamination of glyphosate at neutral pH

Wenning Yang[a,b], *Yangsai Lyu*[c], Ziwei Lan[b], Jia Li[b1], Dickon H.L. Ng[d]

[a]*Shandong Provincial Key Laboratory of Chemical Energy Storage and Novel Cell Technology, School of Chemistry and Chemical Engineering, Liaocheng University, Liaocheng 252000, P. R. China*

[b]*School of Material Science and Engineering, University of Jinan, Jinan 250022, P. R. China*

[c]*Department of Mathematics and Statistics, Queen's University, Kingston, K7L 3N6, Canada*

[d]*School of Science and Engineering, The Chinese University of Hong Kong (Shenzhen), Shenzhen, P. R. China.*

**This file includes Videos S1-S4 and Fig. S1-S5.**



[1]Corresponding authors at: School of Material Science and Engineering, University of Jinan, Jinan, 250022, China.
*E-mail address:* mse_lij@ujn.edu.cn (Jia Li).

## Materials

$ZrOCl_2 \cdot 8H_2O$, $FeCl_3 \cdot 6H_2O$, $Fe(NO_3)_3 \cdot 9H_2O$,1,4-BDC-$NH_2$, dimethylformamide (DMF), NaOH, ethylene glycol (EG), acetic acid (HAc), terephthalic acid (TA), glyphosate, sodium dodecyl sulfonate (SDS, $C_{12}H_{25}SO_3Na$), and $H_2O_2$ (30 wt.%) were purchased from Sinopharm Chemical Reagent Co., Ltd (Shanghai, China). $MnCl_2 \cdot 4H_2O$, $Zr(NO_3)_4 \cdot 5H_2O$ were acquired from Shanghai Macklin Biochemical Co., Ltd (Shanghai, China). Isopropanol (IPA), $NaN_3$, *p*-benzoquinone (BQ), 3,3′,5,5′-tetramethylbenzidine (TMB), o-phenylenediamine (OPD), and 2,2′-azino-bis (3-ethylbenzothiazoline-6-sulfonic acid (ABTS) were supplied by Aladdin Reagent Co., Ltd. (Shanghai, China). *Cynanchum* seed hair was collected in the wild.

## Characterizations

The microstructures of the as-prepared samples was characterized by field emission scanning electron microscopy (FESEM, FEI QUANTA FEG250, USA) and transmission electron microscopy (TEM, JEO-1400, Japan). The elemental composition of samples was identified by energy dispersive X-ray spectroscopy (EDS). The crystal structure of samples was evaluated using X-ray diffraction (XRD) with Cu Kα radiation in the $2\theta$ range of 5° to 80° at a scan speed of $10° \cdot min^{-1}$. Fourier transform infrared (FT-IR) spectra of the prepared samples were tested by a Nicolet 670 FT-IR spectrometer (ThomasNicolet, USA). $N_2$ adsorption/desorption isotherms were measured by a MFA-140 Brunauer-Emmett-Teller (BET) surface analyzer. The fluorescence spectra were determined by an F-7000 fluorescence spectrophotometer (HITACHI, Japan) under the condition of a xenon lamp excitation light source and Ultraviolet-Visible (UV-Vis) absorbance spectra were collected by a UV-3600 plus spectrophotometer (Shimadzu, Japan). Motion videos of micromotors were captured by an optical microscope model (Microscope N-300M, China) with a DC2000 digital camera.

## Experiments

The standard curve of the colorimetric measurements was established according to Equ.S1:

$$\Delta A = A_0 - A \qquad \text{(S1)}$$

where $\Delta A$ is the absorbance variation of oxTMB at 652 nm, $A_0$ and $A$ stand for the absorbance values without and with glyphosate, respectively.

The adsorbed mass per unit mass $q_t$ (mg·g$^{-1}$) at the adsorption time $t$ (min) was calculated according to the following equation:

$$q_t = \frac{(C_0 - C_t)V}{m} \quad \text{(S2)}$$

where $C_0$ (mg·L$^{-1}$) is the initial glyphosate concentration; $C_t$ (mg·L$^{-1}$) is the glyphosate concentration at time $t$ (min); $V$ (L) is the volume of the solution, and $m$ (g) is the mass of the micromotors.

The Michaelis-Menten constant was calculated using a Lineweaver-Burk plot (Equ. S3) (Yang et al., 2019):

$$\frac{1}{v} = \left(\frac{K_m}{V_{\max}}\right)\left(\frac{1}{[S]}\right) + \left(\frac{1}{V_{\max}}\right) \quad \text{(S3)}$$

where $V$ is the initial reaction velocity, $V_m$ is the maximal reaction velocity, [$S$] represents the substrate concentration, and $K_m$ is the Michaelis-Menten constant, which is an indicator of catalyst affinity for its substrate. The smaller the value of $K_m$, the stronger the affinity between the enzyme and the substrate.

The pseudo-first-order kinetic model was drawn as Equ. S4 (Dong et al., 2019):

$$\ln(q_e - q_t) = lnq_e - K_1 t \quad \text{(S4)}$$

where $q_e$ and $q_t$ (mg·g$^{-1}$) are the adsorption capacity (mg·g$^{-1}$) at equilibrium and at any time $t$ (h), respectively, and $K_1$ (h$^{-1}$) is the adsorption rate constant of pseudo-first-order equation. The pseudo-second-order was expressed by the following equation Equ. S5 (Dong et al., 2019):

$$\frac{t}{q_t} = \frac{1}{K_2 q_e^{\,2}} + \frac{1}{q_e}t \quad \text{(S5)}$$

where $K_2$ is the rate constant of the pseudo-second-order model.

The Langmuir isotherm equation was expressed as Equ. S6 (Xun et al., 2015):

$$\frac{C_e}{q_e} = \frac{1}{q_{max}K_L} + \frac{C_e}{q_{max}} \quad \text{(S6)}$$

where $C_e$ (mg·L$^{-1}$) is the equilibrium concentration, and $q_e$ (mg·g$^{-1}$) is the equilibrium adsorption capacity, $q_{max}$ (mg·g$^{-1}$) refers to maximum adsorption capacity. $K_L$ represents the

Langmuir constant. The Freundlich isotherm was given by Equ. S7 (Xun et al., 2015):

$$lnq_e = lnK_F + \frac{1}{n}lnC_e \quad \text{(S7)}$$

where $K_F$ and $n$ are Freundlich constants related to adsorption capacity and adsorption intensity, respectively.

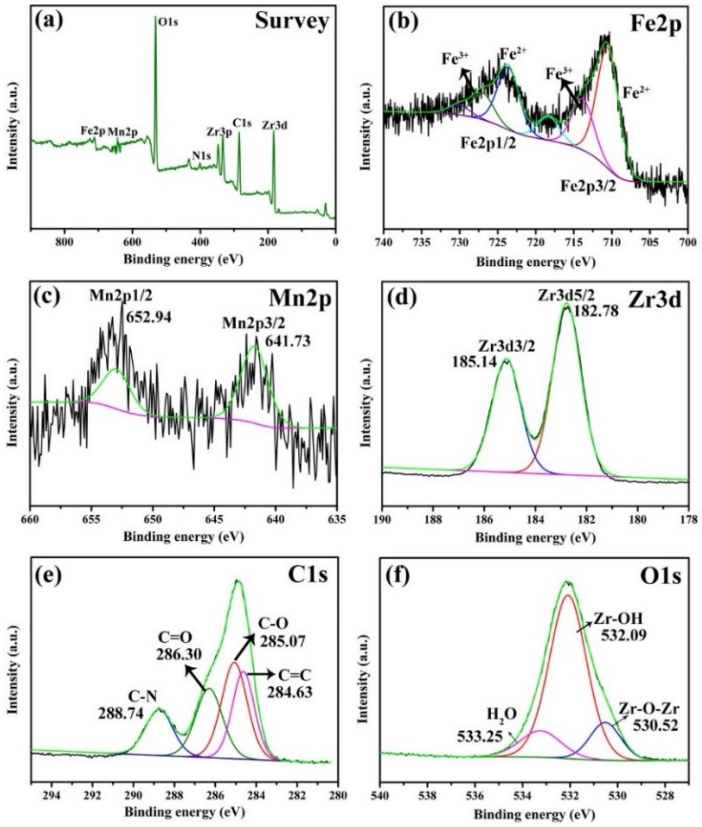


**Fig. S1.** XPS spectra of $ZrO_2$/$MnFe_2O_4$/FeZr-MOF micromotors: survey spectrum (a), and high-resolution spectrum of Fe 2p (b), Mn 2p (c), Zr 3d (d), C 1s (e), and O 1s (f).

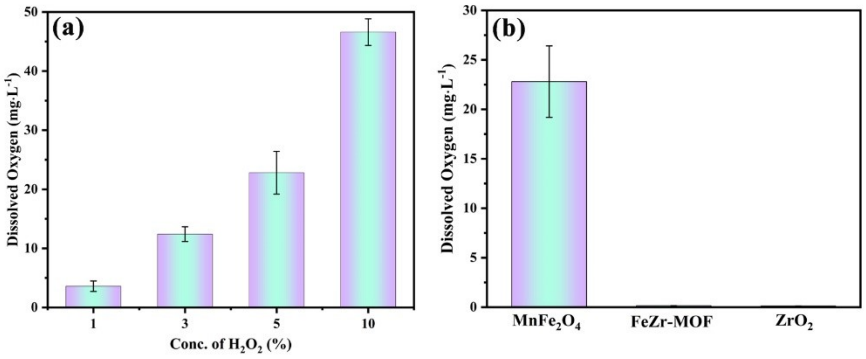


**Fig. S2.** The effect of $H_2O_2$ concentration on the amount of generated $O_2$ (a), and the effect of different catalysts on the amount of generated $O_2$ (b). Error bars represent the standard deviations of three replicate measurements.

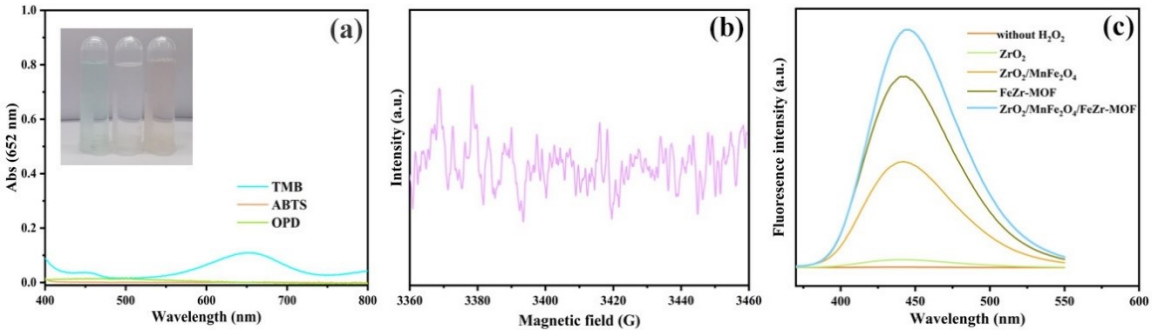


**Fig. S3.** UV-Vis spectra for the oxidation of three substrates catalyzed by $ZrO_2/MnFe_2O_4$/FeZr-MOF without $H_2O_2$ (a), EPR spectrum of DMPO-$O_2^{\bullet-}$ in air saturated solution (b), and the fluorescence spectra of different samples in a basic solution of TA (c).

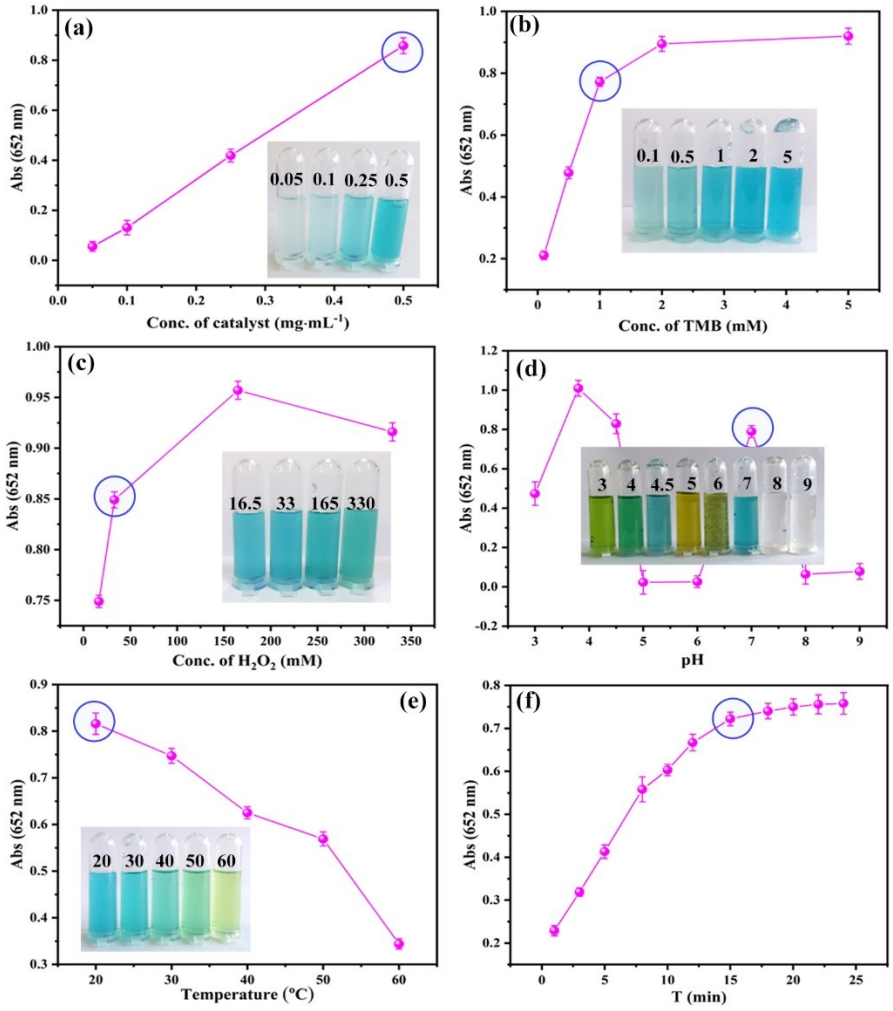


**Fig. S4.** Influence of the micromotors concentration (a), TMB concentration (b), $H_2O_2$ concentration (c), pH value (d), temperature (e), and incubation time (f) on the oxidation of TMB by $ZrO_2/MnFe_2O_4$/FeZr-MOF micromotors. Error bars represent the standard deviations of three replicate measurements.

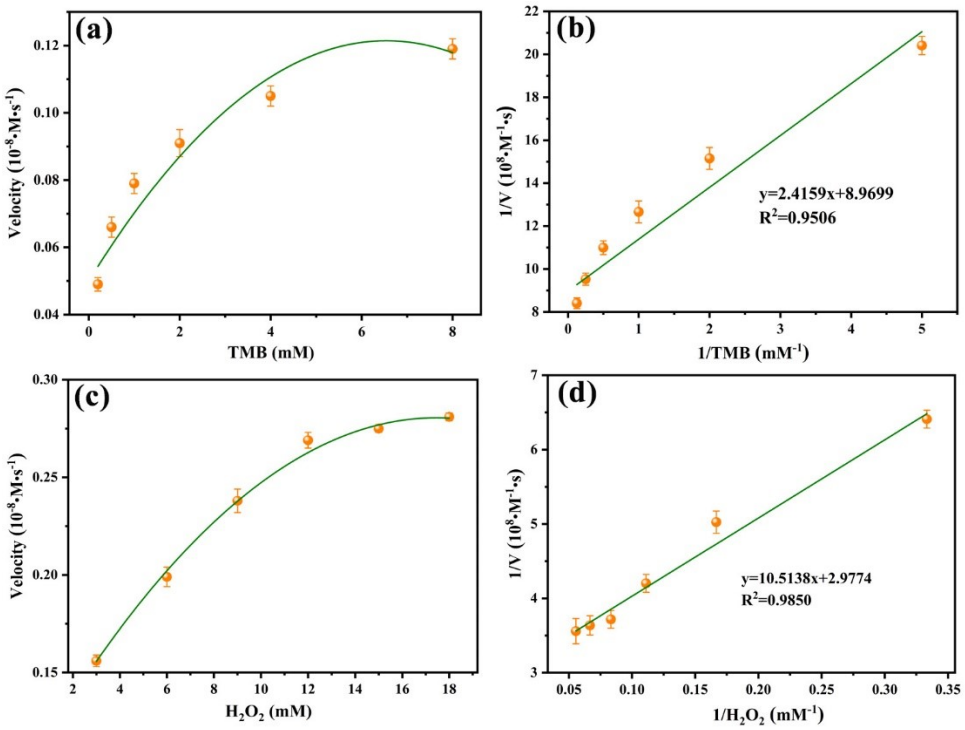


**Fig. S5.** Steady-state kinetic assay (a, c) and the corresponding double reciprocal plots (b, d) of $ZrO_2$/$MnFe_2O_4$/FeZr-MOF micromotors. Error bars represent the standard deviations of three replicate measurements.

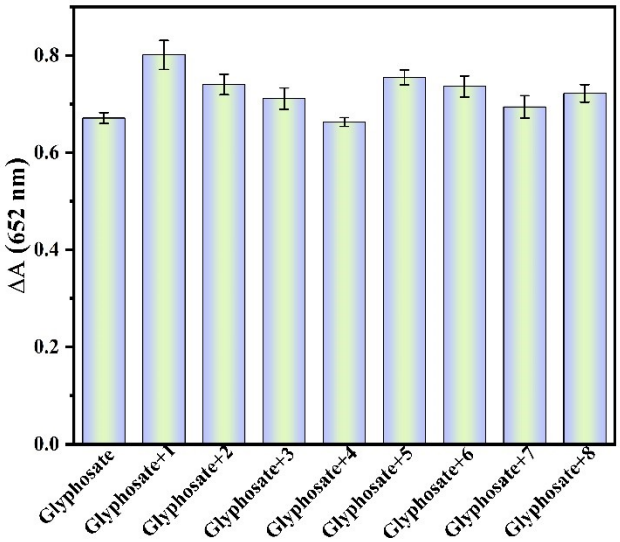


**Fig. S6.** The absorbance variation of oxTMB at 652 nm for the mixture solution of glyphosate and interfering pesticides (1: glufosinate, 2: malathion, 3: acetochlor, 4: atrazine, 5: chlorpyrifos, 6: dimethoate, 7: acetamiprid, 8: carbendazim). Error bars represent the standard deviations of three replicate measurements.

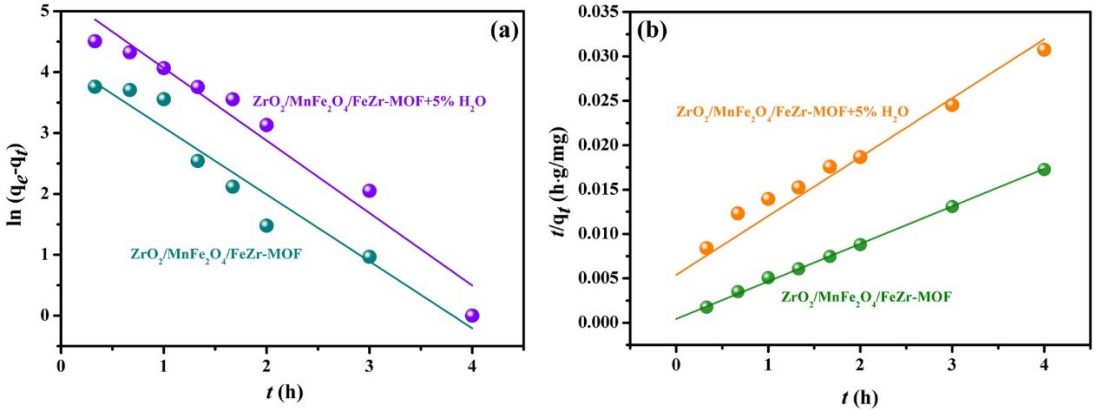


**Fig. S7.** The liner fitting curves of $ZrO_2/MnFe_2O_4$/FeZr-MOF micromotors and non-motors based on pseudo-first-order kinetic model (a) and pseudo-second-order kinetic model (b).

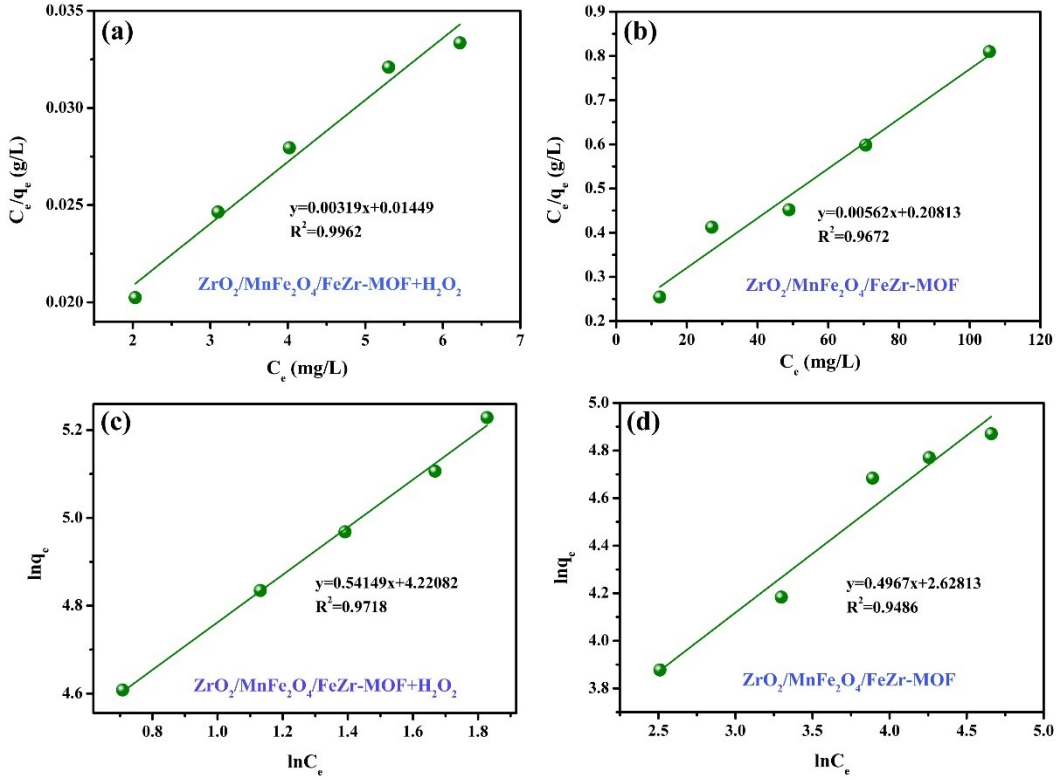


**Fig. S8.** The liner fitting charts of $ZrO_2/MnFe_2O_4$/FeZr-MOF micromotors and non-motors according to Langmuir adsorption isotherm model (a, b) and Freundlich model (c, d).

**Table S1**. Motion parameters of $ZrO_2/MnFe_2O_4$/FeZr-MOF in different concentrations of $H_2O_2$.

| $H_2O_2$ (wt.%) | $L$ (μm) | $a$ (μm) | $U$ (μm·s$^{-1}$) |
|---|---|---|---|
| 3 | 42.8 | 14.1 | 62.3 (1.46 body lengths/s) |
| 5 | 33.9 | 10.1 | 101.6 (3.00 body lengths/s) |
| 10 | 35.2 | 12.7 | 159.8 (4.54 body lengths/s) |

**Table S2**. Comparison of $K_m$ and $V_{max}$ of $ZrO_2/MnFe_2O_4$/FeZr-MOF with other reported materials.

| Catalyst | $K_m$ (mM) | | $V_{max}$ ($10^{-8}$ M·s$^{-1}$) | | Ref |
|---|---|---|---|---|---|
| | TMB | $H_2O_2$ | TMB | $H_2O_2$ | |
| HRP | 0.434 | 3.7 | 10.0 | 8.71 | Yan et al., 2007 |
| $Fe_3O_4$ | 0.285 | 0.238 | 2.91 | 3.21 | Das et al., 2020 |
| [Cu(PDA)(DMF)] | 0.169 | 28.6 | 2.19 | 3.16 | Wang et al., 2019 |
| $NiCo_2O_4$@$MnO_2$ | 2.31 | \ | 127 | \ | Cui et al., 2022 |
| Pt NP@UiO-66-$NH_2$ | 0.127 | 36.5 | 1.36 | 4.15 | Zhang et al., 2017 |
| $Fe_3O_4$@$MnO_2$@ HKUST-1 | 0.317 | 0.322 | 3.07 | 5.08 | Li et al., 2023 |
| $ZrO_2/MnFe_2O_4$/FeZr-MOF | 0.246 | 3.546 | 0.106 | 0.335 | This work |

## References


H. Li, H. Liu, J. Zhang, et al, Platinum nanoparticle encapsulated metal-organic frameworks for colorimetric measurement and facile removal of mercury(II), *ACS Appl. Mater. Interfaces*, 2017, **9**, 40716-40725.

H. Luo, Y. Han, K. Hu, et al, Synthesis of dual function $Fe_3O_4$@$MnO_2$@ HKUST-1 magnetic micromotors for efficient colorimetric detection and degradation of hydroquinone, *New J. Chem.*, 2023, **47**, 1094-1104.

J. Wang, Y. Y. Hu, Q. Zhou, L. Z. Hu, W. S. Fu and Y. Wang, Peroxidase-like activity of metal-organic framework [Cu(PDA)(DMF)] and its application for colorimetric detection of dopamine, *ACS Appl. Mater. Interfaces*, 2019, **11**, 44466-44473.

L. Gao, J. Zhuang, L. Nie, J. Zhang, Y. Zhang, N. Gu, T. Wang, J. Feng, D. Yang, S. Perrett, X. Yan, Intrinsic peroxidase-like activity of ferromagnetic nanoparticles, *Nat. Nanotechnol.*, 2007, **2**, 577-583.

P. K. Boruah, M. R. Das, Dual responsive magnetic $Fe_3O_4$-$TiO_2$/graphene nanocomposite as an artificial nanozyme for the colorimetric detection and photodegradation of pesticide in an aqueous medium, *J. Hazard. Mater.*, 2020, **385**, 17.

Q. Xun, N. Li, S. Yang, et al., A new magnetic nanocomposite for selective detection and removal of trace copper ions from water, *J. Mater. Chem. A* 3, 2015, **3**, 1265-1271.

W. Yang, J. Li, M. Liu, et al., Bioinspired hierarchical CoAl-LDH/$MFe_2O_4$ (Ni,Zn,Co) as peroxidase mimics for colorimetric detection of glucose. *Appl. Clay Sci.*, 2019, **181**, 105238.

Y. Dong, C. Yi, S. Yang, et al., Substrate-free graphene oxide-based micromotor for rapid adsorption of antibiotic, *Nanoscale*, 2019, **11**, 4562-4570.

Y. Ma, M. Zhu, Q. He, M. Zhao and H. Cui, Photoenhanced Oxidase-peroxidase-like $NiCo_2O_4$@$MnO_2$ nanozymes for colorimetric detection of hydroquinone, *ACS Sustain. Chem. Eng.*, 2022, **10**, 5651- 5658.